



## Does liquid slippage within a rough channel always increase the flow rate?

Anna Lee and Ho-Young Kim

Citation: *Physics of Fluids* (1994-present) **26**, 072002 (2014); doi: 10.1063/1.4889740

View online: <http://dx.doi.org/10.1063/1.4889740>

View Table of Contents: <http://scitation.aip.org/content/aip/journal/pof2/26/7?ver=pdfcov>

Published by the [AIP Publishing](#)

---

### Articles you may be interested in

[Eccentricity effects of microhole arrays on drag reduction efficiency of microchannels with a hydrophobic wall](#)  
*Phys. Fluids* **24**, 112004 (2012); 10.1063/1.4767539

[Curvature-induced secondary microflow motion in steady electro-osmotic transport with hydrodynamic slippage effect](#)  
*Phys. Fluids* **23**, 102004 (2011); 10.1063/1.3650911

[On the effects of liquid-gas interfacial shear on slip flow through a parallel-plate channel with superhydrophobic grooved walls](#)  
*Phys. Fluids* **22**, 102002 (2010); 10.1063/1.3493641

[Microchannel flows with superhydrophobic surfaces: Effects of Reynolds number and pattern width to channel height ratio](#)  
*Phys. Fluids* **21**, 122004 (2009); 10.1063/1.3281130

[Slip and accommodation coefficients from rarefaction and roughness in rotating microscale disk flows](#)  
*Phys. Fluids* **19**, 063602 (2007); 10.1063/1.2739416

---



**AIP** | Journal of  
Applied Physics

*Journal of Applied Physics* is pleased to  
announce **André Anders** as its new Editor-in-Chief

## Does liquid slippage within a rough channel always increase the flow rate?

Anna Lee and Ho-Young Kim<sup>a)</sup>

*Department of Mechanical and Aerospace Engineering, Seoul National University, Seoul 151-744, South Korea*

(Received 5 January 2014; accepted 27 June 2014; published online 17 July 2014)

Slippage of liquid over rough superhydrophobic surfaces that induce the Cassie-Baxter state decreases frictional force on the flow. This may easily lead to a hasty conclusion that liquid slip enhances the flow rate in rough channels. Here, we show that flow rates can be rather reduced by roughening and hydrophobizing microchannel walls to support liquid slippage, depending on the topography of the roughness. We consider theoretical models that predict liquid flow rates in channels of different roughness and wetting conditions, to construct criteria for the surface structure that determine whether slip or no-slip would be advantageous in enhancing flow rates. It is shown that liquid slips are advantageous only in channels with highly hydrophobic, short, sparsely distributed protrusions. We corroborate our theoretical predictions with microchannels decorated with micropillars of varying wettabilities. © 2014 AIP Publishing LLC. [<http://dx.doi.org/10.1063/1.4889740>]

### I. INTRODUCTION

Liquid slippage over solid surfaces has long been ignored in macroscale hydrodynamics for its negligible effects on overall flow fields. However, in micro- or nanoscale channels, the slip has been frequently observed experimentally and quantified using a model first proposed by Navier:<sup>1,2</sup>

$$\mathbf{u}_s = b\mathbf{n} \cdot [\nabla\mathbf{u} + (\nabla\mathbf{u})^T], \quad (1)$$

where  $\mathbf{u}$  is the flow velocity,  $\mathbf{u}_s$  is the slip velocity at the solid wall,  $\mathbf{n}$  is the unit vector normal to the wall, and  $b$  is the slip length. While smooth hydrophobic surfaces have been shown to exhibit liquid slip<sup>3-5</sup> presumably due to a liquid depletion layer near the solid surface,<sup>6</sup> the slip length is limited to tens of nanometers, implying insignificant effects on the microfluidic channels whose width or height reaches over tens of micrometers. Since the slip length largely depends on the size of gas pockets on the surface, texturing the hydrophobic solid walls in micro- or nanoscales has been proven to be fairly effective in increasing the slip length up to an order of 100  $\mu\text{m}$ .<sup>7</sup> Because the liquid on rough hydrophobic surfaces slips over the gas layer exerting negligible shear stress, rough hydrophobic walls have been suggested as a potentially viable solution to reduce friction drags for drops<sup>8</sup> and even large vessels.<sup>9</sup>

However, one needs to be cautious in jumping to a conclusion that slippage over rough surfaces is always advantageous in saving energy associated with transporting liquid within channels. The flow rate in channels is a critical function of the cross-sectional area of the fluid stream, which sensitively varies with the surface roughness containing air pockets. The flow rate under the given pressure drop would be enhanced only when the effects of friction reduction dominate over those of shrinkage of stream, which we aim to quantitatively model and corroborate in this study. Nizkaya *et al.*<sup>10</sup> considered the effects of morphology of a textured superhydrophobic wall on the liquid flow. While it was demonstrated that a superhydrophobic trapezoidal channel can be advantageous

<sup>a)</sup> Author to whom correspondence should be addressed. Electronic mail: [hyk@snu.ac.kr](mailto:hyk@snu.ac.kr). Tel.: 82-2-880-9286. Fax: 82-2-880-9287.

in drag reduction and passive mixing compared to that expected for a striped channel, shrinkage of stream caused by air pockets was not addressed. Busse *et al.*<sup>11</sup> considered the flow-blocking effects of superhydrophobic channels by modeling the air pockets as a continuous gas layer. Although the optimal air layer thickness for drag reduction was analytically derived, the results cannot be directly applied to the design of rough surfaces.

In this work, we predict the flow rates in channels whose surfaces are decorated with regularly spaced micropillars. For surfaces with highly hydrophobic pillars inducing the Cassie-Baxter state,<sup>12</sup> the flow rates are given as a function of the slip length that depends on the pillar dimensions. For hydrophilic pillared surfaces achieving the Wenzel state,<sup>13</sup> we consider the velocity fields in the bulk and roughness regions and match them at the boundary of the regions to give the overall flow rates. We also describe the experiments to corroborate our theory.

## II. MODELING

We compare liquid flow rates in the four kinds of two-dimensional channels as shown in Fig. 1—smooth channels I and IV with height  $h$  (a) and  $H = h + k$  (d), respectively, channels II and III decorated with a square array of cylindrical pillars of height  $k$ , diameter  $d$ , and pitch  $l$  (b–c). In channels II and III, the liquid is in the Cassie-Baxter state and the Wenzel state, respectively. For all the channels, the pressure distribution is assumed to be uniform across the channel width and height and to be linear along the channel length. For a pressure-driven flow, the steady-state momentum equation is written as

$$\frac{dP}{dx} = \mu \frac{d^2u}{dy^2}, \quad (2)$$

where  $P$  is the pressure,  $\mu$  is the viscosity of the liquid, and  $u$  is the velocity. The liquid velocity in channel I, obtained by integrating Eq. (2) with no-slip boundary conditions, has the average value of

$$U = -\frac{h^2}{12\mu} \frac{dP}{dx}, \quad (3)$$

and thus the flow rate  $Q$  is  $Uh$ . For channel IV, the dimensionless flow rate,  $\hat{Q} = Q/(Uh)$ , is given by  $\hat{Q} = (1 + \hat{k})^3$ , where  $\hat{k} = k/h$ . When the liquid slips only at the bottom wall as shown in Fig. 1(b), the boundary conditions are such that  $u = b(du/dy)$  at  $y = 0$  and  $u = 0$  at  $y = h$ . The dimensionless velocity in channel II,  $\hat{u} = u/U$ , is obtained as

$$\hat{u} = -6 \left( \hat{y} - \frac{\hat{y} + \hat{b}}{1 + \hat{b}} \right), \quad (4)$$

where  $\hat{y} = y/h$  and  $\hat{b} = b/h$ . The dimensionless flow rate in channel II is then given by

$$\hat{Q} = \frac{1 + 4\hat{b}}{1 + \hat{b}}. \quad (5)$$

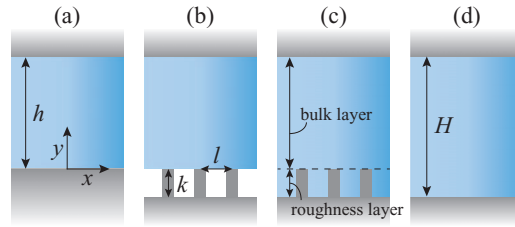


FIG. 1. (a) Smooth channel with height  $h$ . (b) Pillared channel with trapped air pockets that induce the Cassie-Baxter state. (c) Pillared channel under the Wenzel state. (d) Smooth channel with height  $H$ .

TABLE I. The values of  $\alpha$  and  $\beta$  in Eq. (6).

Reference	$\alpha$	$\beta$
14	0.332	0.421
15	0.340	0.468
16	0.325	0.440

The slip length was predicted analytically<sup>14</sup> and numerically<sup>15,16</sup> by assuming zero shear stress on the liquid over gaseous regions and no-slip condition between the liquid and solid. Those studies commonly express  $b$  in the form of

$$\frac{b}{l} = \frac{\alpha}{\sqrt{1-\phi}} - \beta, \quad (6)$$

where  $\phi$  is the surface porosity, or shear-free area fraction, and  $\alpha$  and  $\beta$  are constants. Table I lists the values of  $\alpha$  and  $\beta$  predicted by the previous researchers. Equation (5) implies that measuring  $\hat{Q}$  in channel II, where  $\phi = 1 - (\pi/4)d^2/l^2$ , allows us to obtain the slip length experimentally.

To obtain the analytical expression for the flow rate in the Wenzel state (channel III), we employ a two-layer model proposed by Kuznetsov,<sup>17</sup> where the flow is divided into two layers of the bulk and the roughness layer as shown in Fig. 1(c). Assuming that the flow behavior in the bulk is little disturbed by the roughness, the momentum equation for the bulk layer ( $0 \leq y \leq h$ ) is identical to Eq. (2). In modeling the flow in the roughness layer ( $-k \leq y \leq 0$ ), we note that Ybert *et al.*<sup>16</sup> and Schönecker and Hardt<sup>18</sup> treated a flow of an immiscible fluid enclosed between the solid and main stream liquid. However, the flow of homogeneous fluid is driven by pressure unlike shear-driven flow of the enclosed second fluid. Therefore, we employ the following momentum equation,<sup>19</sup> which includes the pressure term and the drag term due to pillars:

$$\phi \frac{dP}{dx} = \mu \frac{d^2 u_D}{dy^2} - \frac{1}{2} C_d Re_d \frac{\mu u_D}{l^2}, \quad (7)$$

where  $u_D = \phi u$  is the Darcy velocity,  $C_d$  is the drag coefficient, and  $Re_d = \rho u_D l / \mu$  is the local Reynolds number with  $\rho$  being the liquid density. In contrast to previous works<sup>19,20</sup> that obtained  $C_d Re_d$  for an array of square cylinders through numerical simulations, we use the following analytical formula<sup>21,22</sup> of  $C_d Re_d$  for an array of circular cylinders, a geometry adopted in this work:

$$C_d Re_d = \frac{16}{\ln\left(\frac{1}{1-\phi}\right) - \left\{\frac{1-(1-\phi)^2}{1+(1-\phi)^2}\right\}}. \quad (8)$$

The matching conditions at the boundary of the two layers are given by<sup>20</sup>  $u_D(y = -k) = 0$ ,  $u_D(y = 0^-) = u_D(y = 0^+)$ ,  $\mu \frac{du}{dy}(y = 0^-) = \mu \frac{du}{dy}(y = 0^+)$ , and  $u(y = h) = 0$ . By integrating Eqs. (2) and (7) with the matching and boundary conditions, the dimensionless velocity can be obtained as

$$\hat{u}_D = \phi \left\{ \frac{12}{A} + B \cosh(\sqrt{A}\hat{y}) + D \sinh(\sqrt{A}\hat{y}) \right\} \quad (9)$$

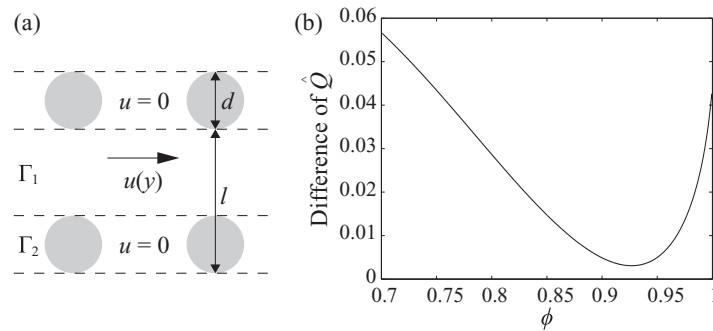


FIG. 2. (a) Schematic illustration of the top view of liquid flow in the roughness region assumed in the simple model. (b) The difference in dimensionless flow rates,  $\hat{Q}$  from Eq. (14) minus  $\hat{Q}$  from Eq. (13).

for  $-\hat{k} \leq \hat{y} \leq 0$ , and

$$\hat{u}_D = 6(1 - \hat{y}^2) + \sqrt{AD}(\hat{y} - 1) \quad (10)$$

for  $0 \leq \hat{y} \leq 1$ . Here,  $A = C_d Re_d / (2\hat{l}^2)$  with  $\hat{l} = l/h$ ,  $C = \cosh(\sqrt{A}\hat{k})$ ,  $S = \sinh(\sqrt{A}\hat{k})$ ,

$$B = \frac{6}{A} \left\{ \frac{-2\sqrt{A} + (A - 2\phi)S}{\sqrt{AC} + \phi S} \right\}, \quad (11)$$

$$D = \frac{6}{A} \left\{ \frac{2\phi + (A - 2\phi)C}{\sqrt{AC} + \phi S} \right\}. \quad (12)$$

By integrating Eq. (9) from  $-\hat{k}$  to 0 and Eq. (10) from 0 to 1, the dimensionless flow rate of channel III is given by

$$\hat{Q} = 4 - \frac{1}{2}\sqrt{AD} + \frac{\phi}{\sqrt{A}}(D + BS - DC) + 12\frac{\hat{k}\phi}{A}. \quad (13)$$

Motivated by the idea of dividing the flow region into two, we investigate whether a simpler model for the flow in channel III yields a similar result to Eq. (13). Assuming that the liquid can pass through the gaps of pillars with the velocity profile identical to that in smooth channel IV, while completely blocked by the pillars as schematically illustrated in Fig. 2(a), the flow rate of channel III is the sum of the flow rate in the region free of pillars (area  $\Gamma_1$ ),  $\hat{Q}_{\Gamma_1} = (1 + \hat{k})^3(1 - \hat{d}/\hat{l})$ , and that in the pillared region (area  $\Gamma_2$ ),  $\hat{Q}_{\Gamma_2} = \hat{d}/\hat{l}$ :

$$\hat{Q} = \frac{\hat{d}}{\hat{l}} + (1 + \hat{k})^3 \left( 1 - \frac{\hat{d}}{\hat{l}} \right). \quad (14)$$

Figure 2(b) plots the difference between the flow rates of channel III obtained by Eqs. (13) and (14). The difference between the dimensionless flow rates does not exceed 6% within the ranges typically allowable in microfluidic channels, revealing that the simple model is often sufficient to evaluate quickly the effects of hydrophilic protrusions on the flow rate.

### III. EXPERIMENTAL

To corroborate the theoretical model, we measure the liquid flow rates in various microchannels as shown in Fig. 3, which consist of etched glass and silicon wafers. A glass wafer is wet-etched to shape a channel of 30  $\mu\text{m}$ , 1 mm, and 20 mm in depth, width, and length, respectively. The high ratio of the channel width to depth allows us to assume a two-dimensional flow, justifying the foregoing theoretical approach. To provide the inlet and outlet to the straight channel, holes 2 mm in diameter are formed mechanically on both ends of the channel. For a pillar-structured surface, a silicon wafer

TABLE II. Contact angles ( $\theta$ ) for the surfaces prepared in the experiments. The standard deviation is  $\sim 1^\circ$ .

Surface	$\theta$ (deg)
Piranha cleaned, smooth	5
Piranha cleaned, pillared	$\sim 0$
OTS coated, smooth	105
OTS coated, pillared	166

is deep-reactive-ion etched, leaving a square array of cylindrical pillars of  $6 \mu\text{m}$  height ( $k$ ) and 3, 4, 5, 6, or  $7 \mu\text{m}$  in diameter ( $d$ ). The distance between the centers of each pillar,  $l$ , is always  $12 \mu\text{m}$ . The glass wafer containing the channel and the smooth or pillared silicon wafer constituting a base are aligned and anodically bonded.

We test three different types of surfaces: smooth hydrophilic, pillared hydrophilic, and pillared superhydrophobic. Piranha cleaning is carried out for every channel to remove organic residues, which hydrophilizes the channels. For the superhydrophobic surface, the piranha-cleaned channel walls are coated with octadecyltrichlorosilane (OTS) as follows. First, a 5-mM OTS solution in hexadecane is brought into the channel. After 2 h, the channel is rinsed by flowing hexane followed by methanol and dried by flowing nitrogen gas.<sup>23</sup> Then, the channel is baked on a hot plate at  $100^\circ\text{C}$  for 2 h. The contact angles between deionized (DI) water drops ( $5 \mu\text{l}$  volume) on piranha-cleaned and OTS-coated silicon wafer surfaces, both smooth and pillared, are obtained by measuring the angle between the tangential lines of the liquid interface and the solid surface at the contact line. The contact angles for each surface are listed in Table II. As shown in Fig. 4, the pillared superhydrophobic surface achieves the Cassie-Baxter state with water, whereas the pillared hydrophilic surface induces the Wenzel state. The topological properties of the microchannels yield values of 0.2 for  $\hat{k}$ , 0.4 for  $\hat{l}$ , and 0.8–0.95 for  $\phi$ .

A plastic tube and a glass capillary with a 2-mm inner diameter are attached with epoxy to the inlet and outlet of the channel, respectively. The microchannel is initially filled with DI water. Then, 3450 Pa of air pressure is applied to the inlet of the channel using a pump (ONIX microfluidic perfusion system, CellASIC Corporation) to transport liquid towards the outlet. To measure the water flow rate, the changes of water level at the outlet capillary are recorded using a high-speed camera

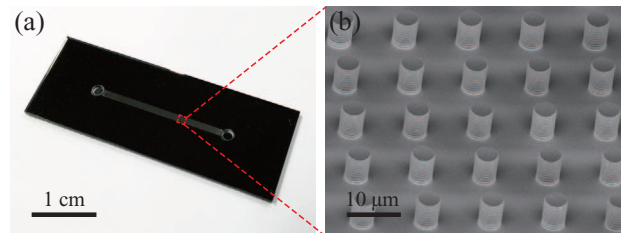


FIG. 3. (a) Optical image of a microchannel. (b) Scanning Electron Microscopy (SEM) image of a channel base decorated with an array of micropillars.

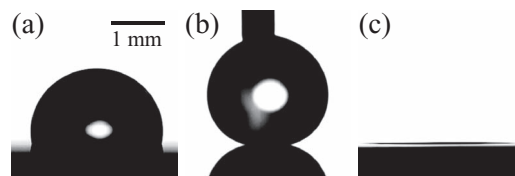


FIG. 4. (a) A water drop on the OTS-coated smooth Si surface. (b) A water drop on the OTS-coated pillared Si surface with  $k = 6 \mu\text{m}$ ,  $d = 5 \mu\text{m}$ , and  $l = 12 \mu\text{m}$ . (c) A water drop on the piranha-cleaned pillared Si surface with  $k = 6 \mu\text{m}$ ,  $d = 5 \mu\text{m}$ , and  $l = 12 \mu\text{m}$ .

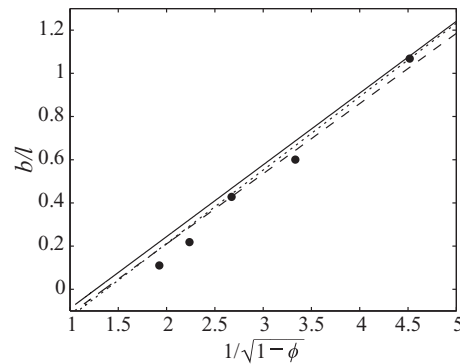


FIG. 5. Comparison of the effective slip lengths,  $b/l$ , experimentally measured and theoretically predicted as a function of  $\phi$ . The dashed line corresponds to the model of Ybert *et al.*,<sup>16</sup> the dotted line to Ng and Wang,<sup>15</sup> and the solid line to Davis and Lauga.<sup>14</sup>

(FASTCAM APX RS, Photron) at the frame rate of  $60 \text{ s}^{-1}$ . The flow rate is obtained by multiplying the rate of change in the water level and the inner cross-sectional area of the glass capillary.

#### IV. RESULTS AND DISCUSSION

We first compare the theoretical predictions of  $b$  in Table I and the experimental results for  $b$  calculated from Eq. (5) with measured  $\hat{Q}$  in channel II, in Fig. 5. We experimentally confirm that the slip length linearly increases with  $1/\sqrt{1-\phi}$ . Overall, the model by Ybert *et al.*<sup>16</sup> exhibits the smallest error when compared with the experimental results although all the three predictions showed reasonable agreement with experiment. In the following, we use  $\alpha = 0.325$  and  $\beta = 0.440$  in Eq. (6), as suggested by Ybert *et al.*, to evaluate  $b$ .

We compare the theoretically predicted velocity profiles in the four different kinds of the channels in Fig. 6. For the flows within the forest of pillars (i.e., roughness layer) occurring in channel III, we plot the Darcy velocity. For all the porosity  $\phi$ , the velocity is lower in channel III than in channel IV because of the drag and reduced flow area due to the pillars. The velocity is always higher in channel II than in channel I owing to the slip at the bottom. As  $\phi$  increases, the velocity in channel II increases rapidly along with the slip length, whereas the velocity in channel III increases but slightly. Furthermore, the velocity in channel II surpasses that in channel IV for  $0 < \hat{y} < 1$  as  $\phi$  exceeds approximately 0.9, Fig. 6(b). The maximum dimensionless velocity in channel II reaches 2.49 for  $\phi = 0.95$ , which is 1.66 times higher than that of channel I.

We now consider how effectively flow rates can be enhanced starting from channel I, by roughening (channels II and III) or simply enlarging (channel IV) the channel. The dimensionless flow rate  $\hat{Q}$  scaled by the flow rate in channel I corresponds to the flow rate enhancement ratio. We plot the theoretical values of  $\hat{Q}$  for channels II, III, and IV with varying  $\phi$  in Fig. 7. We see that  $\hat{Q}$  of channel IV is always higher than that of channel III, meaning that simply expanding the channel area is more effective in enhancing flow rates than roughening channels to induce the Wenzel state. Comparing  $\hat{Q}$  of the rough channels II and III, the flow rate in channel III (Wenzel state) is higher than that in channel II (Cassie-Baxter state) for  $\phi < 0.84$  in the current channels with  $\hat{k} = 0.2$  and  $\hat{l} = 0.4$ . It is only for  $\phi > 0.84$  that  $\hat{Q}$  in channel II exceeds  $\hat{Q}$  in channel III. Even in this range,  $\hat{Q}$  in channel IV is higher than that in channel II until  $\phi$  reaches 0.93.  $\hat{Q}$  of channel II is the highest only for  $\phi > 0.93$ . We also show the experimental results in Fig. 7, measured for channels II and III with different pillar dimensions, which follow the same tendency as the theory predicts.

The results in Fig. 7 imply that it is better for flow rate enhancement to remove the surface roughness (to make the channel height  $H$  from  $h$ ) than to hydrophobize the rough surface (to induce liquid slippage) unless the porosity is extremely high. Even for the same rough channel surfaces (channels II and III), the Wenzel state is more advantageous in improving the flow rate than the Cassie-Baxter state up to a very high porosity. In short, the liquid slippage over rough channel

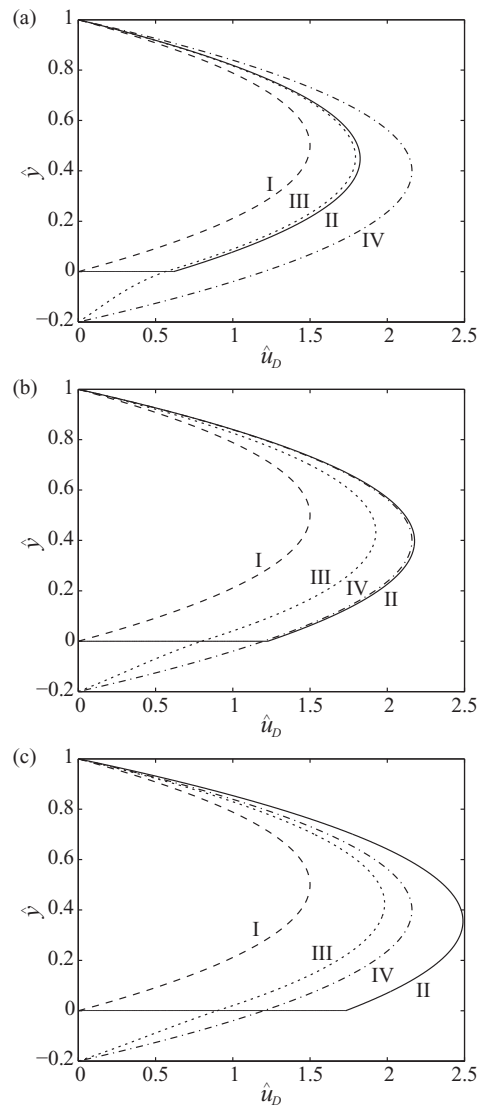


FIG. 6. Dimensionless velocity profiles with (a)  $\phi = 0.8$ , (b)  $\phi = 0.91$ , and (c)  $\phi = 0.95$ .

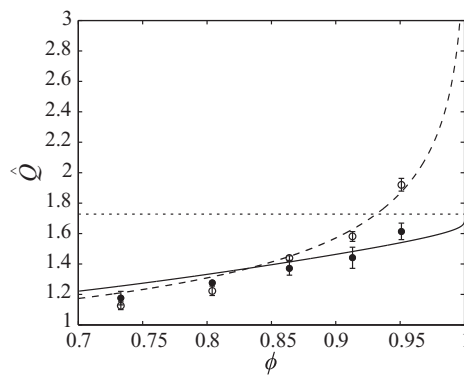


FIG. 7. Comparison of the experimental results and the theoretically predicted flow rate enhancement ratio in the Cassie-Baxter (empty circles and dashed line, respectively) and Wenzel states (filled circles and solid line, respectively). The dimensionless flow rate in the smooth channel with height  $H$  is represented by the dotted line.

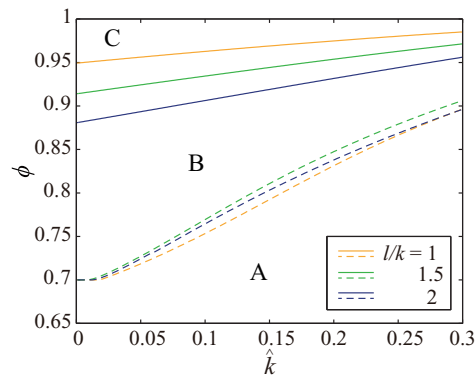


FIG. 8. The dashed lines indicate the conditions where the flow rates in the Cassie-Baxter and Wenzel state channels are equal. The solid lines display the conditions where the flow rate in the Cassie-Baxter state channel and the smooth channel with height  $H$  are identical. In regimes A, B, and C,  $\hat{Q}_{II} < \hat{Q}_{III} < \hat{Q}_{IV}$ ,  $\hat{Q}_{III} < \hat{Q}_{II} < \hat{Q}_{IV}$ , and  $\hat{Q}_{II} < \hat{Q}_{IV} < \hat{Q}_{III}$ , respectively. Here  $\hat{Q}_{II}$ ,  $\hat{Q}_{III}$ , and  $\hat{Q}_{IV}$  are the dimensionless flow rates in channels II, III, and IV, respectively.

surfaces increases the flow rate compared to those in hydrophilic rough channels and expanded smooth channels only when the porosity is considerably high, which we have quantified here.

As  $\hat{Q}$  is a function of  $\hat{k}$  and  $\hat{l}$  as well as  $\phi$ , we can calculate which wetting state would be more advantageous in increasing the flow rate for given pillar dimensions. The results are shown in Fig. 8, where we plot the boundaries of each regime. In regime A, the flow rate is higher in the Wenzel state (channel III) than in the Cassie-Baxter state (channel II). The flow rate is higher in the Cassie-Baxter state than in the Wenzel state in regimes B and C. In regimes A and B, the flow rate is the highest for the channel widened (channel IV) instead of that roughened. It is only in regime C, with very high  $\phi$  and small  $\hat{k}$ , that the Cassie-Baxter state inducing liquid slippage is the most effective in increasing the flow rate. We also vary the values of pitch  $l$  scaled by pillar height  $k$ , to find the delicate effects of  $l/k$  on the regime boundaries. Overall, to take advantage of slip for increasing the flow rate, the channel surface should be decorated with short, slender, and sparse pillars so that the slip length and porosity can be maximized.

It is well known, however, that the array of sparsely distributed, short, and slender pillars is vulnerable to transition from the Cassie-Baxter to the Wenzel state because the liquid suspended on the pillar tops can easily invade into the gaps between the pillars. The transition of the wetting state is likely to occur when either the meniscus hanging from the tips of the pillars touches the substrate bottom or the meniscus starts to slide down the pillar side as the contact angle exceeds the critical advancing contact angle,  $\theta_A$ .<sup>24,25</sup> Such deformation of menisci is caused by the increase in liquid pressure that bulges the interface. Balancing the capillary force with the pressure force, the critical pressure corresponding to the meniscus touching the bottom is given by<sup>24</sup>

$$\Delta P_{c,1} = \frac{8(1-\phi)k\gamma}{\phi d^2}, \quad (15)$$

where  $\Delta P$  is the pressure difference between liquid and trapped air and  $\gamma$  is the surface tension coefficient. The critical liquid pressure that causes the contact angle to reach  $\theta_A$  is written as<sup>24</sup>

$$\Delta P_{c,2} = \frac{4(1-\phi)}{\phi} |\cos \theta_A| \frac{\gamma}{d}. \quad (16)$$

As the liquid pressure is the highest at the channel inlet, the driving pressure should be carefully chosen to prevent the Wenzel state in the beginning. Once the Cassie-Baxter state is established, it is likely to be sustained downstream as the pressure decreases along the length of the channel. Comparing the values of  $\Delta P_{c,1}$  and  $\Delta P_{c,2}$  for our experimental conditions, we find that  $\Delta P_{c,2} = 1750$  Pa is smaller than  $\Delta P_{c,1} = 20410$  Pa. Thus, the water may slide down rather than touch the bottom when liquid pressure exceeds  $\Delta P_{c,2}$ . We also note that the critical pressure can be enhanced by a factor of 4 for  $\phi > 0.9$  due to the compression of air trapped on the surface that helps stabilize the

Cassie-Baxter state.<sup>26</sup> On this account, it is likely that the Cassie-Baxter state has been established near the entrance of channel II in our experiments.

## V. CONCLUSIONS

We have investigated the effects of the wetting state on the velocity profile and rate of liquid flow in pillared microchannels. Theoretically predicted velocity is always higher in the Cassie-Baxter state than in the Wenzel state. It is theoretically predicted and experimentally corroborated that when the porosity is small and pillar heights are large, the flow rate in the Wenzel state exceeds that in the Cassie-Baxter state. Inducing slip serves to effectively increase liquid flow rate only for a large porosity and short pillars. Although our analysis deals with two parallel plates, one smooth and the other roughened, one can easily extend the results to two parallel rough plates (even to circular tubes). With the boundary condition at the upper surface changed to  $du/dy = 0$  corresponding to the center plane between the plates, we find that the boundaries of the regimes as displayed in Fig. 8 are modified only slightly (within  $\pm 3\%$ ). While hydrophobic rough channels with small slip lengths may be disadvantageous to the flow rate, the slipping flows near the solid surfaces can be effectively used for some microfluidic applications. In particular, the absence of slow-moving fluid near the wall would give advantage in controlling axial dispersion of analytes in microchannels.<sup>27</sup> The criteria developed and verified in this work can guide a design of microfluidic channels used in various applications including lab-on-a-chip systems<sup>28</sup> and heat-exchangers of HVACR (Heating, Ventilation, Air-Conditioning, and Refrigeration) apparatus<sup>29</sup> to maximize the flow rate under given channel size and pumping pressure.

## ACKNOWLEDGMENTS

This work was supported by the National Research Foundation of Korea (Grant No. 2014023206) funded by the Korea government via SNU-IAMD.

- <sup>1</sup> C. L. M. H. Navier, "Mémoire sur les lois du mouvement des fluides," *Mem. Acad. Sci. Inst. Fr.* **6**, 389–440 (1823).
- <sup>2</sup> E. Lauga and H. A. Stone, "Effective slip in pressure-driven Stokes flow," *J. Fluid Mech.* **489**, 55–77 (2003).
- <sup>3</sup> S. Jin, P. Huang, J. Park, J. Y. Yoo, and K. S. Breuer, "Near-surface velocimetry using evanescent wave illumination," *Exp. Fluids* **37**, 825–833 (2004).
- <sup>4</sup> L. Joly, C. Ybert, and L. Bocquet, "Probing the nanohydrodynamics at liquid-solid interfaces using thermal motion," *Phys. Rev. Lett.* **96**, 046101 (2006).
- <sup>5</sup> P. Joseph and P. Tabeling, "Direct measurement of the apparent slip length," *Phys. Rev. E* **71**, 035303 (2005).
- <sup>6</sup> J. P. Rothstein, "Slip on superhydrophobic surfaces," *Annu. Rev. Fluid Mech.* **42**, 89–109 (2010).
- <sup>7</sup> C. Lee, C.-H. Choi, and C.-J. Kim, "Structured surfaces for a giant liquid slip," *Phys. Rev. Lett.* **101**, 064501 (2008).
- <sup>8</sup> J. Kim and C.-J. Kim, "Nanostructured surfaces for dramatic reduction of flow resistance in droplet-based microfluidics," in *Proceedings of the IEEE Conference on MEMS, Las Vegas, NV* (IEEE, 2002), pp. 479–482.
- <sup>9</sup> S. L. Ceccio, "Friction drag reduction of external flows with bubble and gas injection," *Annu. Rev. Fluid Mech.* **42**, 183–203 (2010).
- <sup>10</sup> T. V. Nizkaya, E. S. Asmolov, and O. I. Vinogradova, "Flow in channels with superhydrophobic trapezoidal textures," *Soft Matter* **9**, 11671–11679 (2013).
- <sup>11</sup> A. Busse, N. D. Sandham, G. McHale, and M. I. Newton, "Change in drag, apparent slip and optimum air layer thickness for laminar flow over an idealised superhydrophobic surface," *J. Fluid Mech.* **727**, 488–508 (2013).
- <sup>12</sup> A. B. D. Cassie and S. Baxter, "Wettability of porous surfaces," *Trans. Faraday Soc.* **40**, 546–551 (1944).
- <sup>13</sup> R. N. Wenzel, "Resistance of solid surfaces to wetting by water," *Ind. Eng. Chem.* **28**, 988–994 (1936).
- <sup>14</sup> A. M. J. Davis and E. Lauga, "Hydrodynamic friction of fakir-like superhydrophobic surfaces," *J. Fluid Mech.* **661**, 402–411 (2010).
- <sup>15</sup> C.-O. Ng and C. Y. Wang, "Apparent slip arising from Stokes shear flow over a bidimensional patterned surface," *Microfluid. Nanofluid.* **8**, 361–371 (2010).
- <sup>16</sup> C. Ybert, C. Barentin, C. Cottin-Bizonne, P. Joseph, and L. Bocquet, "Achieving large slip with superhydrophobic surfaces: Scaling laws for generic geometries," *Phys. Fluids* **19**, 123601 (2007).
- <sup>17</sup> A. V. Kuznetsov, "Analytical investigation of the fluid flow in the interface region between a porous medium and a clear fluid in channels partially filled with a porous medium," *Appl. Sci. Res.* **56**, 53–67 (1996).
- <sup>18</sup> C. Schönecker and S. Hardt, "Longitudinal and transverse flow over a cavity containing a second immiscible fluid," *J. Fluid Mech.* **717**, 376–394 (2013).
- <sup>19</sup> G. Gamrat, M. Favre-Marinet, S. Le Person, R. Bavière, and F. Ayela, "An experimental study and modelling of roughness effects on laminar flow in microchannels," *J. Fluid Mech.* **594**, 399–423 (2008).

- <sup>20</sup>R. Bavière, G. Gamrat, M. Favre-Marinet, and S. Le Person, "Modeling of laminar flows in rough-wall microchannels," *J. Fluids Eng.* **128**, 734–741 (2006).
- <sup>21</sup>J. Happel, "Viscous flow relative to arrays of cylinders," *AICHE J.* **5**, 174–177 (1959).
- <sup>22</sup>A. Tripathi and R. P. Chhabra, "Transverse laminar flow of non-Newtonian fluids over a bank of long cylinders," *Chem. Eng. Commun.* **147**, 197–212 (1996).
- <sup>23</sup>C.-H. Choi, K. J. A. Westin, and K. S. Breuer, "Apparent slip flows in hydrophilic and hydrophobic microchannels," *Phys. Fluids* **15**, 2897–2902 (2003).
- <sup>24</sup>D. Bartolo, F. Bouamrine, É. Verneuil, A. Buguin, P. Silberzan, and S. Moulinet, "Bouncing or sticky droplets: Impalement transitions on superhydrophobic micropatterned surfaces," *Europhys. Lett.* **74**, 299–305 (2006).
- <sup>25</sup>T.-G. Cha, J. W. Yi, M.-W. Moon, K.-R. Lee, and H.-Y. Kim, "Nanoscale patterning of microtextured surfaces to control superhydrophobic robustness," *Langmuir* **26**, 8319–8326 (2010).
- <sup>26</sup>P. Forsberg, F. Nikolajeff, and M. Karlsson, "Cassie-Wenzel and Wenzel-Cassie transitions on immersed superhydrophobic surfaces under hydrostatic pressure," *Soft Matter* **7**, 104–109 (2011).
- <sup>27</sup>D. Dutta and D. T. Leighton, "Dispersion reduction in pressure-driven flow through microetched channels," *Anal. Chem.* **73**, 504–513 (2001).
- <sup>28</sup>H. A. Stone, A. D. Stroock, and A. Ajdari, "Engineering flows in small devices: Microfluidics toward a lab-on-a-chip," *Annu. Rev. Fluid Mech.* **36**, 381–411 (2004).
- <sup>29</sup>H. A. Mohammed, G. Bhaskaran, N. H. Shuaib, and R. Saidur, "Heat transfer and fluid flow characteristics in microchannels heat exchanger using nanofluids: A review," *Renewable Sustainable Energy Rev.* **15**, 1502–1512 (2011).